Geomechanics and Engineering, *Vol. 31, No. 6 (2022) 599-614*
https://doi.org/10.12989/gae.2022.31.6.599

Experimental evaluation of back-to-back anchored walls by double-plates anchors

Amir Najafizadeh[a] and AmirAli Zad*

Department of Civil Engineering, Faculty of Civil & Earth Resources Engineering, Islamic Azad University, Central Tehran Branch, Tehran, Iran

(*Received June 24, 2022, Revised November 24, 2022, Accepted December 14, 2022*)

Abstract. One of the methods of stabilizing retaining walls, embankments, and deep excavations is the implementation of plate anchors (like the Geolock wall anchor systems). Back-to-back Mechanically Stabilized Earth (BBMSE) walls are common stabilized earth structures that can be used for bridge ramps. But so far, the analysis of the interactive behavior of two back-to-back anchored walls (BBAW) by double-plates anchors (constructed closely from each other and subjected to the limited-breadth vertical loading) including interference of their failure and sliding surfaces has not been the subject of comprehensive studies. Indeed, in this compound system, the interaction of sliding wedges of these two back-to-back walls considering the shear failure wedge of the foundation, significantly impresses on the foundation bearing capacity, adjacent walls displacements and deformations, and their stability. In this study, the effect of horizontal distance between two walls (W), breadth of loading plate (B), and position of vertical loading was investigated experimentally. In addition, the comparison of using single and equivalent double-plate anchors was evaluated. The loading plate bearing capacity and displacements, and deformations of BBAW were measured and the results are presented. To evaluate the shape, form, and how the critical failure surfaces of the soil behind the walls and beneath the foundation intersect with one another, the Particle Image Velocimetry (PIV) technique was applied. The experimental tests results showed that in this composite system (two adjacent-loaded BBAW) the effective distance of walls is about W = 2.5*H (H: height of walls) and the foundation effective breadth is about B = H, concerning foundation bearing capacity, walls horizontal displacements and their deformations. For more amounts of W and B, the foundation and walls can be designed and analyzed individually. Besides, in this compound system, the foundation bearing capacity is an exponential function of the System Geometry Variable (SGV) whereas walls displacements are a quadratic function of it. Finally, as an important achievement, doubling the plates of anchors can facilitate using concrete walls, which have limitations in tolerating curvature.

Keywords: back-to-back walls; BBAW walls; bearing capacity; failure surface; interaction; Particle Image Velocimetry (PIV); retaining walls; shallow foundation; sliding surface; system geometry

1. Introduction

One of the methods of anchoring retaining walls in excavation sides (under the structures' foundations loads) and the bridge abutments (under roads' traffic loads), etc. is the implementation of anchor plates. Also, Nowadays, the use of Back-to-Back Mechanically Stabilized Earth (BBMSE) walls has received special attention due to economic consideration and ease of implementation. But so far, extensive studies have not been developed considering the evaluation of the compound system of two back-to-back anchored walls (BBAW) by anchor plates, and under a load of shallow foundation. Therefore, previous studies are mentioned regarding each part in the following.

1.1 BBMSE walls

BBMSE walls are one of the kinds of so-called "stabilized earth with complex geometry" due to their geometry and loading conditions. The FHWA-NHI-10-024 devotes its sixth chapter to the design and construction of mechanically stabilized earth walls and reinforced soil slopes to this kind of walls (Ryan *et al*. 2009). According to this Code (based on Elias and Christopher (1997), Elias *et al.* (2001) researches), if the distance between two walls is more than the value of (H.tan(45-φ/2)) (H is the height of each wall and φ is the angle of soil internal friction), the back-to-back walls are far enough far from each other and can be analyzed and designed without interfering the active and reinforcement zones. This distance was introduced as the Effective Distance (Ryan *et al.* 2009).

One of the important parameters in the design of BBMSE walls considering lateral forces behind the walls is a determination of the angle of the sliding surface. This angle indicates the geometry of the slipped wedge, which puts pressure on the back of the wall (Niroumand and Kassim 2016).

Won and Kim (2007) investigated the changes in lateral pressure behind the back of each wall, the horizontal displacement of walls, and the maximum tensile stress of

*Corresponding author, Assistant Professor
E-mail: a.zad@iauctb.ac.ir
[a]Ph.D.
E-mail: amirnajafizadeh1@gmail.com

ISSN: 2005-307X (Print), 2092-6219 (Online)

reinforcements. The wall was reinforced with single-layer geogrids. Based on the results of this study, it was observed that when the distance between the walls reinforced zones (S) is equal to the height of the wall, the lateral pressure behind the walls is approximately equal to the active pressure calculated using the Rankin method. However, the amount of soil pressure increases in the lower quarter of the wall and reaches the soil pressure at rest, and this is due to the fixity of the wall toe within the rigid base (a generalization of the effect of boundary conditions is a function of strength and hardness of the soil at the toe of the wall). It was also concluded that the critical sliding surfaces of the back-to-back walls at a distance S greater than the wall height do not intersect. This indicates that for BBMSE walls with a larger S or equal in height, they act independently from each other and can be analyzed as individual walls. The collision and superposition of critical sliding surfaces begin when the distance S is less than the height of the walls. Also, reducing the wall distance S causes the approach of critical slip surfaces towards the walls which leads to a reduction in the slip wedge volume. Furthermore, the conclusions of this study showed that the maximum tensile value for each reinforcement layer on top of the wall is the lowest and increases accordingly with an increase in the depth of the reinforcement layer. In general, maximum tension occurred in the reinforcement layers in the middle third of the wall. The amount of tension force decreases by moving to the lower quarter of the wall height.

In the research by Han and Leszczynski (2010), the location and the shape of the critical slip surface of BBMSE walls -reinforced by steel strips- were determined at different ratios of the distances of the facings of the walls to the height of each wall (W/H). Based on their research, the shear stress intensity contours in the numerical method showed that the critical slip surfaces of two walls do not interfere with each other in W/H ratios greater than 2. Also, comparing the position and shape of the critical slip surface in different W/H ratios with the characteristics of the backfill soil can explain how the critical slip surface does not enter the reinforced area of the opposite wall. Although for W/H=1.4, the position and shape of the critical slip surface transforms and enters the reinforcement zone of the opposite wall.

El-Sherbini *et al*. (2013) studied the effect of the distance between two BBMSE walls and the internal friction angle (φ) of the wall's backfill soil on the maximum tensile stress of the reinforcements (geogrid). The results indicated that two BBMSE walls system with two different soils properties (φ=25°,30°) have a different effect on one another in each case and the maximum stress appears in the lower third of the wall height for the soils with high internal friction angle materials and two thirds for the low internal friction angle materials. It should be noted that the maximum stress in the upper part of the wall with a ratio of W/H=1.4 is slightly higher than the walls with W/H=2 and W/H=3 ratios. This result can be explained by the fact that the maximum reinforcement tensile stress of the BBMSE walls with a ratio of W/H=1.4 is spread to both back sides of the walls and is formed by overlapping the slip surface in the upper part, therefore the stresses in the upper part of the wall increase.

Taghizadeh *et al.* (2016) also studied the effects of the distance between two BBMSE walls by changing the soil internal friction angle (φ) and the connection of reinforcements on the soil slip surface angle using numerical modeling. They concluded that in a specified wall (in terms of height and type), the angle of the soil slip surface increases with increasing the soil internal friction angle (φ). It was shown that this relation is established in all the cases of wall distances (a single line, 2-lines, and 3-lines roads) for both connected and disconnected cases. Also, in a wall with a constant backfill height, for different walls distances (1-line, 2-lines, and 3-lines roads), the ratio of soil slip surface angle decreases with increasing wall distance. In addition, in BBMSE walls, the slip surface angle of two walls due to the height of the wall and the internal friction angle of the soil can intersect with each other and therefore should be designed simultaneously. Meanwhile, the angle of the slip surfaces changes and increases from the intersection. In BBMSE walls, if the slip surfaces of walls are non-intersecting, each of them acts individually and has no effects on each other, and can be analyzed and designed independently.

Benmebarek and Djabri (2017) carried out numerical modeling using the finite element method (FEM) to analyze the behavior of Geosynthetic-Reinforced BBMSE walls under harmonic cyclic stresses. To study the seismic response, numerical modeling was developed in a plain-strain mode using PLAXIS 2D. The results were evaluated in terms of horizontal displacements of back-to-back walls and tensile loads on the reinforcements (maximum reinforcement stress) at the end of each cyclic harmonic loading. The results showed that if the distance between two walls is reduced (case W/H=1.4), the maximum horizontal displacement will decrease significantly. This sharp decrease in wall displacements was attributed to the interaction of walls constructed closely together. The reduction of displacement in near-distance walls indicates that if the distance between two walls is severely reduced, these BBMSE walls can be designed with a higher degree of reliability for general global stability. It was also observed that for all of the studied W/H ratios in dynamic conditions, the distribution of the maximum tensile stress of reinforcements is linear. This result was similar to that presented in previous studies for the mechanically stabilized earth walls (MSEW) with simple geometry on one side.

In the general view, the past studies were focused on the BBMSE walls (under a distributed load) distance effects on the wall's angle of soil sliding wedges, horizontal displacements, horizontal forces distribution, and also, maximum tensile stress in reinforcements (Steel Strips s or Geogrids). But, the back-to-back anchored walls (BBAW) especially under limited-breadth load like a railway or shallow foundation have not been considered a lot.

1.2 Anchor plates

Plate anchors are one of the soil reinforcement elements which are composed of a buried-in-soil backer plate with an anchor rod or strand to transfer wall lateral force to the soil.

In developed countries, these mechanical plate anchors are widely used and have many applications for foundations, retaining walls, storage tanks, floating offshore platforms, buried and submerged pipelines, and many other engineering applications (Das 2014). These days, various types of Plate anchors are used onshore and offshore including horizontal, inclined, and vertical plate Anchors, frictional anchors, load-bearing vertical friction anchors, buried suction plate anchors, and dynamic intrusion anchors (Niroumand and Kassim 2016, Jalali Moghaddam *et al*. 2021).

In this case, Jalali Moghadam *et al*. (2019) studied the performance of plate anchors in retaining walls and their influences on the three parameters of dimensions, shape, and arrangement of restraining plates based on the experimental evaluation. The results showed that plates with larger dimensions are more efficient than small and medium dimensions. Also, circular plates in both categories of bearing capacity of loading plate and wall displacement had a better performance than square plates. However, due to the small differences in the efficiency of the square and circular shapes (the results showed that the effect of the shape of the plate anchors geometry (circular and square) on the control of horizontal displacement is less than 5%) and due to the difficulty of implementing round restraint plates, these types of plates have been selected as the optimal mode in the present study and were used in modeling. Also, the 4-anchor rhombus arrangement in the facade in front of the wall has a better performance than the 4-anchor square arrangement in the facade in front of the wall, and considering that the rhombus arrangement has one less anchor than the five-anchor arrangement, therefore, it can be a better option than both of them. Moreover, double-plates anchors have not been the subject of extensive studies yet and in this study, these kinds of anchors are applied.

1.3 Compound system

Finally, the objectives of this article are to present and analyze the experimental evaluation results (physical modeling) of the architectural features (horizontal distance of two walls, the breadth of the loaded shallow foundation) influences on the shallow foundation bearing capacity, walls horizontal displacements and deformations and also on the composite failure surfaces formations mechanism and their shapes. To observe the critical composite failure surfaces (and the shape of the failure wedge of the walls) of BBAW, the Particle Image Velocimetry (PIV) technique was applied.

2. Experimental program

A scale of 1 to 10 was applied to perform experiments on a laboratory scale and to construct BBAW. Accordingly, all prototype dimensions were divided by the number 10. Therefore, for a wall with a height of 5 meters, the height of the experimental model was reduced to 50 cm. Also, this scaling factor was applied to other dimensions as well.

To study the influence of walls distances on the behavior of BBAW, 4 distances including 110 cm, 120 cm, 130 cm, and 140 cm were specified and to evaluate the influence of loading plate breadth, 4 breadths including 10 cm, 20 cm, 30 cm, and 50 cm were considered for the experimental Program.

It should be noted that embracing two back-to-back walls by connecting their anchor rods leads to the formation of a structural bending frame with fixed joints. Also, to stabilize and strengthen these types of systems under dynamic loads, the required components and connections to fix using the braces to tolerate bending moments. However, both of the above-mentioned methods are expensive and unjustifiable, and therefore not applicable in practice.

2.1. Material used

For modeling a retaining wall, which is mainly made of prefabricated steel or concrete or monolithic concrete sections, Wood (2004) conducted a dimensional analysis and introduced four types of materials with different thicknesses to be used in the 300 mm concrete facing in the laboratory model (Table 1). In this study, a 0.9 mm-thick aluminum plate was used in the experimental tests (Wood 2004).

In Table 1 E_m, tm is the thickness and hardness of the equivalent material to a concrete wall 30 cm thick, respectively. Accordingly, in all experiments, an aluminum sheet with a thickness of 0.9 mm was used.

In all the experiments, sand extracted from the Sufyan region in East Azerbaijan province in Iran was used, which according to previous studies was identified as a suitable type of soil for PIV analysis (The grains of this reflect different color spectrums which differentiate the grains in the captured images).

Table 1 Equivalent materials for modeling a 300 mm-thick concrete facing (Wood 2004)

Facing material	Elastic modulus, E_m (GPa)	Thickness, t_m (mm)
Steel	210	0.64
Aluminum	70	0.9
Micro-concrete	10	1.75
Polypropylene	0.9	3.9

Table 2 Physical and mechanical properties of the soil

Parameter	Index	Unit	Amount
USCS Classification	-	-	SP
Uniformity Coefficient	C_u	-	1.34
Curvature Coefficient	C_c	-	1.89
Effective Grain Size	D_{10}	mm	0.25
Mean Grain Size	D_{50}	mm	0.31
Internal Friction	φ	Degree	30
Cohesion		kPa	~0
Specific Gravity	G_s	-	2.65

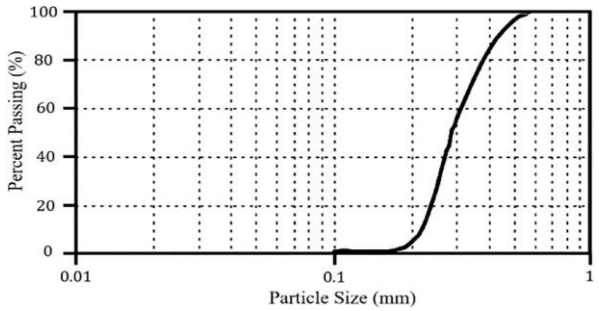

Fig. 1 Soil Particle Size Distribution graph for experimental tests

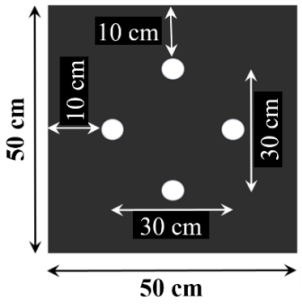

Fig. 2 Front view of anchors arrangement in the walls (Jalali Moghadam *et al.* 2019)

The physical and mechanical characteristics of this soil are presented in Table 2 and its Particle Size Distribution graph is shown in Fig. 1. The strength properties were obtained from a Direct Shear test according to ASTM D 3080-04 (2004) (Table 2).

2.2 Experimental tests configuration using double-plate anchors

Commonly, Commonly, in most anchored retaining walls construction, the horizontal and vertical distances of the anchors have a minimum and a maximum size of 1 to 2 meters from each other. For active reinforcements which are post-tensioned, such as cables and monobars (for example soil nails), the horizontal and vertical distances should satisfy these limitations. Whereas the horizontal and vertical distances of passive anchors (i.e., not post-tensioned), such as the grouted and helical (screw) soil nails, were previously reported to be 1000 to 3000 mm (Sabatini *et al.* 1999, Perko 2009, Lazarte *et al*. 2015).

According to Jalali Moghadam *et al.* (2019) research, the most optimal arrangement of anchors is a diagonal distance of about 3 m for horizontal distances and 3 m for vertical distances of anchors and by applying a 1:10 scale factor to this dimension, the value of 30 cm for the distance from the center to the center of the anchors in the walls was obtained. Fig. 2 shows a schematic plan of the 4 rhombus anchors used in this study (Jalali Moghaddam *et al.* 2018, Jalali Moghaddam *et al*. 2019).

The slip failure wedges of walls were evaluated based on Rankine's theory. The experimental test results showed that the minimum length for the plate anchors to be placed outside the failure wedge was 400 mm. But promising results were achieved by selecting a length of 500 mm for the reinforcements to embed the plate anchors in the passive zone of the wall. This will keep them sufficiently far from the failure wedge to deal with the lateral soil pressure**.** The two sides of the tie rods were threaded to the plate anchors and the wall facing, respectively. According to the scale ratio of 1:10, plates with 25 mm length (double-plate anchor length is equivalent to 50 mm length single-plate anchor) were used.

The length of the rods was 50 cm, and the reduced scale of the 5-meter rods was achieved by applying a 1 to 10 reduction factor. Also, their diameter is equal to 4 mm, which was equivalent to an anchor rod with a diameter of 4 cm (rebar ϕ40) in practice. The plate anchor in this research was of the square type, which became 2.5 cm for each plate using a 1:10 scale factor. Fig. 3 displays a sample of the plate anchor along with an anchor rod for experimental tests.

2.3 Instrumentation and data acquisition system

To make laboratory samples and based on the explanations provided in the dimensional analysis section, a chamber 170 cm long, 50 cm wide, and 80 cm deep was built. The larger amount of chamber length and depth was due to prevent the occurrence of boundary effects on the test results and the width of the chamber was selected to 50 cm, equal to the length of the wall, to ensure the complete establishment of plane strain conditions.

To capture the soil deformations during performing the tests using camera snapshotting, one side of the chamber was made of transparent glass with a suitable thickness of 3 cm was installed. This thickness was used to ensure that it will not be deformed during loading in the experiments. Tognon *et al.* (1999) placed polyethylene plastic sheets on the walls of a box to minimize the friction angle between the walls and soil to less than 5 degrees (Tognon *et al.* 1999).

To apply the simulated load of a shallow foundation, rigid steel plates with different breadths were used and was tried to follow Plate Load Test conditions based on ASTM compound system mechanical behavior (measurement of deformation versus loading). Also, to achieve the highest possible accuracy and constant loading rate in all tests, the linear-strain loading method was used. Due to this approach, a linear variable differential transformer (LVDT) was installed on the movable shaft of the loading system, so that the loading can be applied with the same increment in each step and the loading speed was kept constant at around 1 mm/min. Also, a load cell was used to record the amount of force applied during the loading steps. All data, including loading and settlement of footings loads, were recorded by a digital data logging system (Data Logger). Also, to measure the deformation of the walls, three linear variable differential transformers (LVDT) were installed at the height level of the walls. D 1195 to record the Using a Galaxy S8 camera with a charge-coupled device (CCD) sensor and 10-megapixel shooting power, the walls were photographed at the end of each loading step, and then the

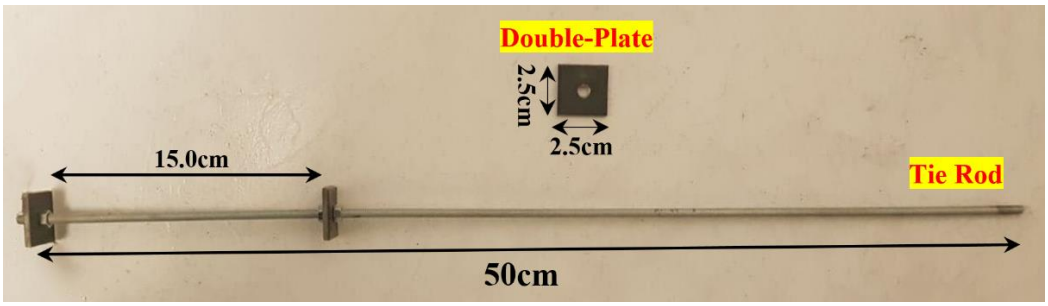

Fig. 3 Used sample tie rods and plate anchors

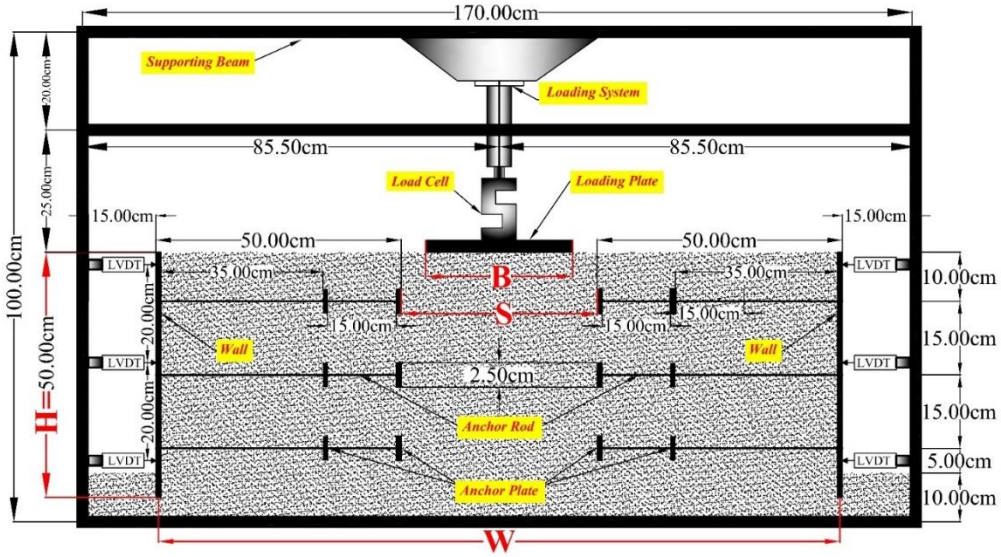

Fig. 4 The schematic shape of the physical modeling apparatus

displacement of soil particles was determined using PIV (Particle Image Velocimetry) analysis method between consecutive images.

Fig. 4 shows the test chamber, loading system, and performed instrumentation, along with the dimensions and location of plate anchors.

2.4 Experimental procedure

In general, the process of walls construction is the same in all experiments and consists of the stages of backfilling, compaction, installation, and placement of anchors at any height level. Accordingly, the backfilling of each layer was implemented from the bottom of the chamber and was continued until it reaches the target level. By installing the facing in the designated place, the anchors were installed and connected to the facings. Both sides of the rods were threaded to be connected to the plate anchors on one side and the facing on the other side through the embedded holes. Then, with the filling and compacting of the soil layers behind the walls and reaching the level of installation of the upper anchors, their installation and connection to the facings were repeated. Finally, by filling the chamber until reaching the top of the walls, the construction of the retaining wall was completed. The thickness of each layer was kept constant by 5 cm and compaction was conducted in both ponding and vibration until the desired level of a layer reaches a constant density in experiments with a target soil unit weight.

Each test was performed in 50 steps (50 mm settlement of loading plate). During the constant loading plate settlement ratio of one millimeter and continuous recording of the applied load, the loading plate settlement and the horizontal displacements of the walls were recorded by the data logger, and the soil particle movement was captured by taking a photo. This process was continued in a total of 50 steps to reach the 5 cm loading plate settlement. Table 3 describes all the 12 performed experimental tests and their characteristics.

3. Results

As mentioned before, the bearing capacity values of the loading plate and walls displacements in three soil levels were recorded for all the experimental tests, continuously by Data Logger. In this study, the settlement of 50 mm is considered as the Ultimate Limit State (ULS) to the specification of the bearing capacity values to ensure of steady hardening ratio of the pressure-settlement curve (Fig. 5). Moreover, since in this study the complex failure surfaces should be survived, thus ensuring their completion, 50 mm settlement is considered as the ULS (Najafizadeh *et al.* 2022).

Table 3 Experimental test results using double-plate anchors

Test	Test Index	Back-to-Back Walls Distances	Loading Plate Breadth	Bearing Capacity at 5 cm settlement	Maximum Horizontal Displacement at 5 cm Settlement
No.	-	W	B	Q	h
-	-	cm	cm	kPa	mm
1	D-110-10	110	10	34.75	6.13
2	D-110-20	110	20	40.19	11.61
3	D-110-30	110	30	46.92	18.22
4	D-110-50	110	50	55.80	27.90
5	D-120-10	120	10	37.93	7.48
6	D-120-20	120	20	43.48	13.30
7	D-120-30	120	30	49.36	19.92
8	D-120-50	120	50	59.40	29.08
9	D-130-10	130	10	45.74	10.42
10	D-130-20	130	20	51.00	15.31
11	D-130-30	130	30	56.33	22.08
12	D-130-50	130	50	63.37	31.45
13	D-140-10	140	10	56.55	7.96
14	D-140-20	140	20	59.53	17.50
15	D-140-30	140	30	62.97	25.07
16	D-140-50	140	50	67.71	34.26

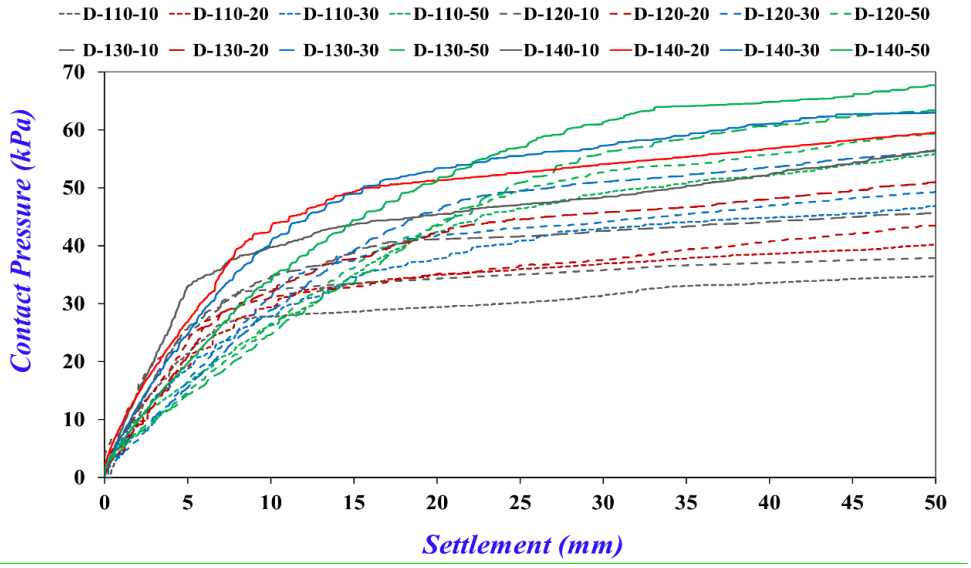

Fig. 5 All the tests loading plate contact pressures versus settlement

Table 3 presents the bearing capacity values of the loading plate with different breadths and different distances of the back-to-back walls anchored by double-plate anchors.

3.1 Theoretical approach

In this complex system of two BBAW anchored walls loaded by a shallow foundation, there are two slip failure surfaces of walls and one shear failure surface of shallow foundation will occur (Fig. 6.). The formation of each of them and its interaction with others can lead to different failure behavior and different form of the composite failure surface. From the theoretical point of view, there are two composite modes of interference and failure as a result of that (Fig. 6);

- **Mode I**; The first mode is the interference of one side of the loading plate shear surface with that side wall slip failure surface that causes the formation of a new, compound, and superposed surface that is called "*Composite Failure Surface*" since now.
- **Mode II**; The second mode is interference and interaction of the two composite failure surfaces (mode I.) of walls. It should be noted that Mode II just when happens that Mode I happened before. Otherwise, Mode II. is meaningless.

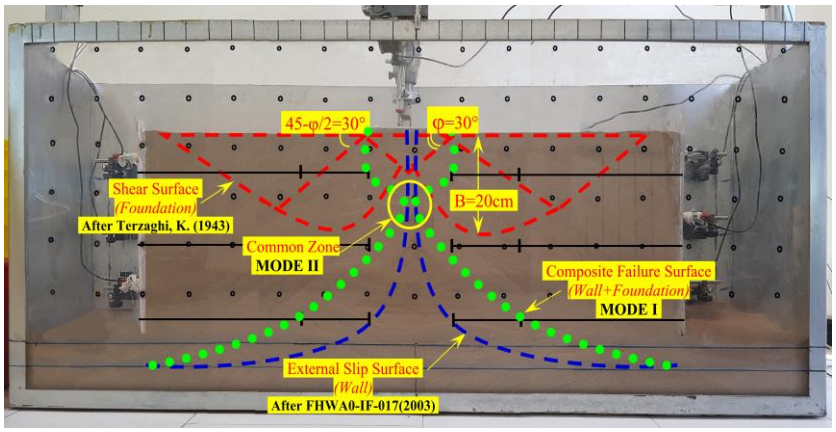

Fig. 6 Compound system schematic failure modes related to the D-120-20 test. (walls sliding failure surfaces (Lazarte *et al*. 2015), loading plate shear fracture surfaces (Terzaghi 1943), and composite failure surfaces)

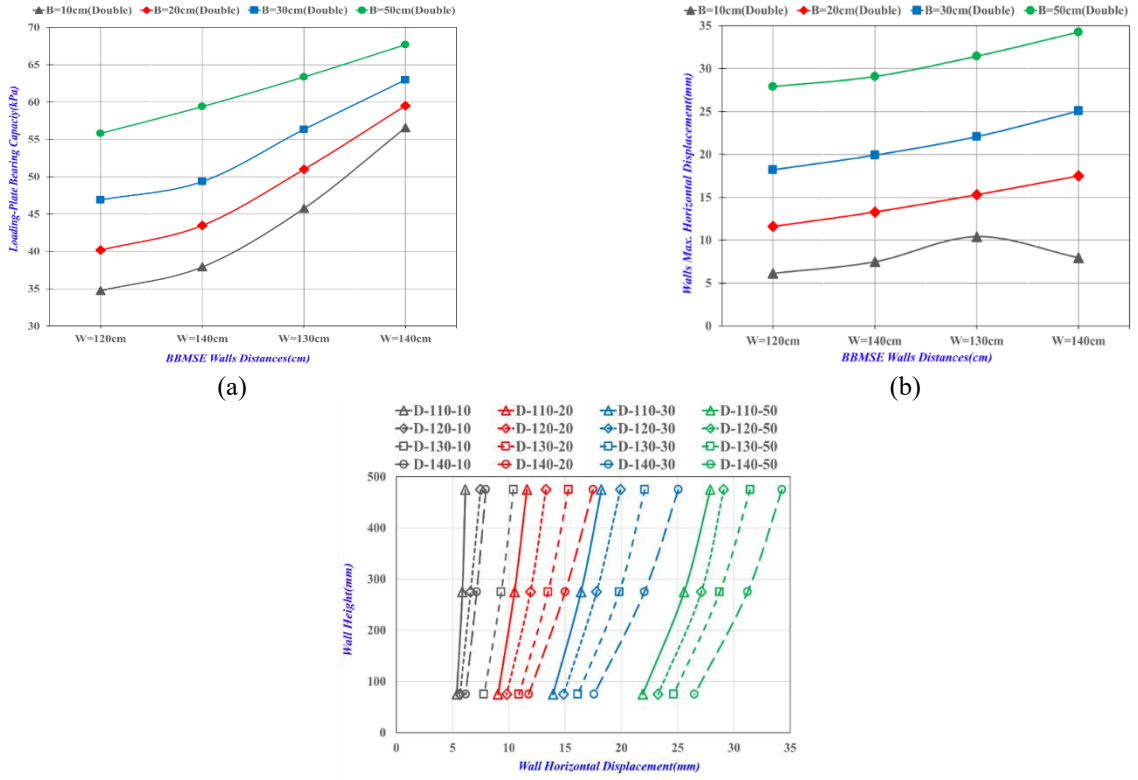

Fig. 7 Effect of back-to-back walls distances on loading plate bearing capacity, walls head displacements, and walls deformations

Fig. 6 shows the general overview of the modeling apparatus with the location and approximate position of the slip-wedges surfaces of the walls embankments (Lazarte *et al.* 2015) and the shear failure surfaces of the soil under the loading plate (Terzaghi 1943). Also, the composite failure surfaces, studied in this article by application of the PIV technique, are shown in green ellipses in Fig. 6.

Since complex failure surfaces and their interactions are visible when Ultimate Limit State (ULS) happens and the stress-strain behavior enters the plastic zone, therefore in this study (regarding the indication of compound system failure surfaces), all the bearing capacities amounts were considered in 10% of wall height, equivalent 5 cm to be ensured of occurrence of complete plastic behavior and getting to constant hardening ratio of the compound system.

4. Discussion

4.1 Influence of walls distance

In this section, the effect of walls horizontal distances on the loading plate bearing capacity, walls maximum horizontal displacement, and their deformations are considered (Fig. 7.).

A comparison of loading plates' bearing capacity

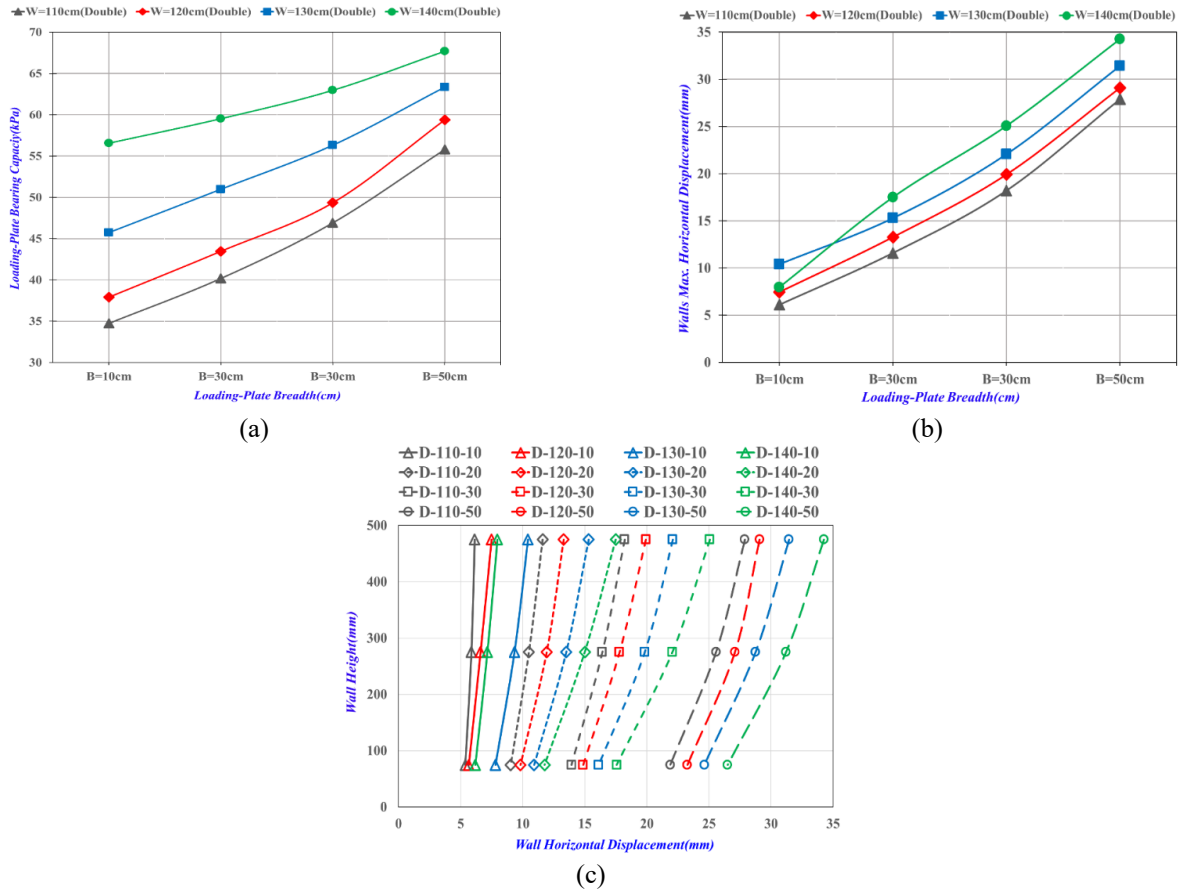

Fig. 8 Effect of Loading plate breadth on its bearing capacity, walls head displacements, and walls deformations

diagrams versus their settlements (Fig. 7(a)) shows the increase in walls distances increases the bearing capacity. Based on the results, a 10 cm increment in walls distances leads to 8%, 18%, and 22% growth in bearing capacity for 120, 130, and 140 cm of walls distances respectively. Also, the gradient of walls maximum horizontal displacements against loading plate settlement (Fig. 7(b)) indicates a direct relation between these two parameters. Analyzing the relation of them shows that a 10 cm increment in walls distances from 110 cm to 140 cm results on average about 13%, 21%, and 3% increase, respectively, except for D-140-10. It seems this exception is related to the lack of wall slip surfaces (It is discussed in PIV analysis in section 4.6).

Fig. 7(c) demonstrates that the increase in walls distance leads to both curvature and tilting of the walls but from their comparison, it is inferred that tilting is the dominant behavior.

4.2 Influence of loading plate breadth

In this section, the walls back-to-back distances are kept constant and for the different breadth of the loading plates, their bearing capacity, walls horizontal displacements, and their deformative behaviors are analyzed (Fig. 8).

The gradient of loading plates' bearing capacity diagrams versus their settlements (Fig. 8(a)) shows that a 10 cm increment of the loading plate breadth from 10 cm to 50 cm causes loading plate bearing capacity to increase about 12%, 13%, and 19% respectively. A comparison of walls maximum horizontal displacements graphs versus loading plate settlement (Fig. 8(b)) presents that a 10 cm increment in the loading plate breadth from 10 cm to 50 cm results in walls maximum horizontal displacement on average about 83%, 91%, and 121% respectively.

The deformation of walls demonstrated in Fig. 8(c) through walls horizontal displacement in three levels, shows that increasing the loading plate breadth leads to curvature and tilting but the comparison of deformations presents that increasing the loading plate breadth causes much more tilting than curvature.

4.3 B/S Ratio

To investigate the influence of foundation location between two walls reinforced zone, the B/S ratio was defined and its effect on bearing capacity and horizontal displacements were studied. This variable presents the ratio of two back-to-back walls plate anchors to loading plate breadth (B and S parameters are shown in Fig. 4). This ratio can represent the intense interactive behaviors among two walls and the loading plate on each other, which is explained graphically in the PIV test results (section 4.6).

In this section, the relations between the bearing capacity of the loading plate and the walls maximum horizontal displacement are analyzed (Fig. 9).

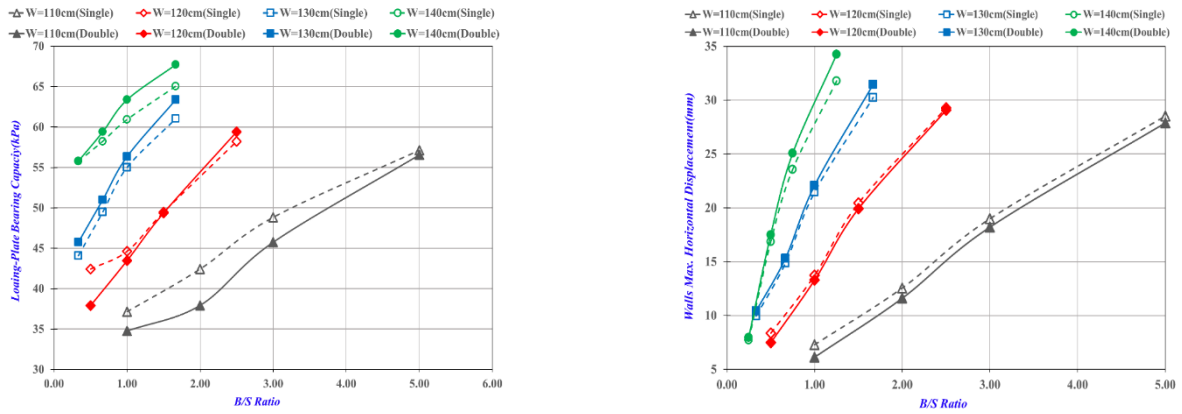

(a) (b)

Fig. 9 Effect of B/S ratio on its bearing capacity, walls heads displacements, and walls deformations

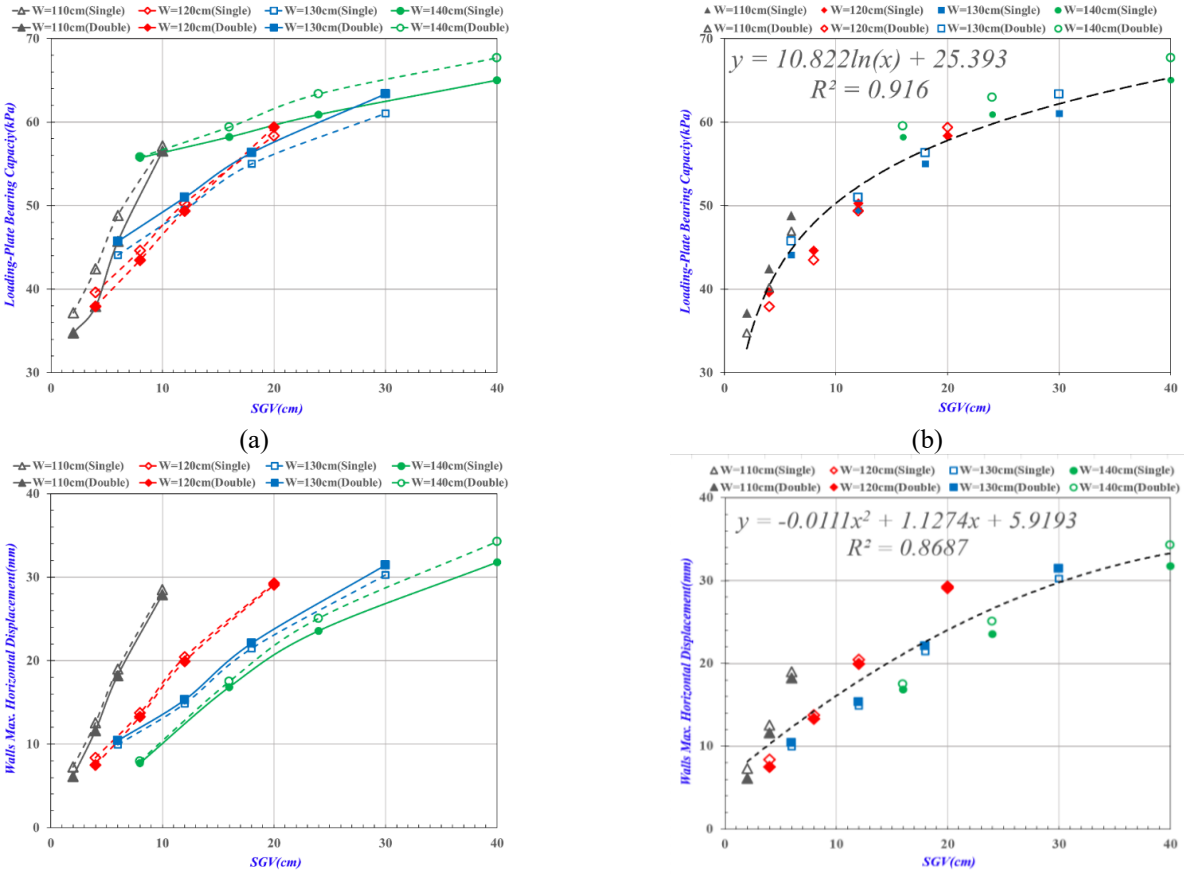

(a) (b)

(c) (d)

Fig. 10 Effect of System Geometry Variable (SGV) on its bearing capacity and walls heads displacements

Also, the influence of the S/B ratio on the form of composite failure surfaces is discussed in the PIV analysis in section 4.6. It should be mentioned the data of previous author studies related to single-plates anchors are added to scrutinize the compound system behavior more precisely.

The gradient of loading plates bearing capacity (Fig. 9(a)) and walls maximum horizontal displacement (Fig. 9(b)) diagrams versus S/B ratio shows by increasing the S/B ratio, both of them increase directly. This relation is linear and shows the sensitivity of compound system bearing capacity and horizontal displacement to this ratio.

4.4 System Geometry Variable (SGV)

Since for shallow foundations without any interaction with retaining walls, the bearing capacity (based on the Terzaghi's relation, its terms are soil cohesion ($c.N_c$), embedment ($\gamma.D_f.N_q$), and footing breadth ($\gamma.B.N_\gamma/2$) (Terzaghi 1943)) and the settlement (immediate settlement relation) are directly related and dependent to its geometrical features, Therefore, for the shallow foundation with interaction to retaining walls, specification of the relation of geometrical features and shallow foundation

bearing capacity and walls displacement is necessary. According to the importance of specifying a logical and mathematical relationship between geometrical parameters and measured parameters, many factors, ratios, and variables were tried to achieve a comprehensive and useful relationship among mentioned issues. Finally, the System Geometry Variable (SGV) was chosen as the best in a sign of geometrical affecting parameters (Eq. (1))

$$SGV = \frac{B(cm)*D(cm)}{H(cm)} \quad (1)$$

Where (as shown in Fig. 4);
B: Loading plate breadth
D: Back-to-back plate anchors distances
H: Back-to-back walls height

Although this variable can be used to model loading plate bearing capacity and walls maximum horizontal displacement numerically. However, it seems when walls and loading plate do not have interaction and interference or when walls internal slip surfaces are active will not work very well. Therefore, in the following procedure two tests results including B=10 cm, W=140 cm, and B=50 cm, W=110 cm were eliminated from regression (It is discussed in PIV results in section 4.6). In Fig. 10 the changes in the procedure of loading plate bearing capacity and walls horizontal distances versus SGV are shown.

As is shown in Figs. 10(b), 10(d) the relationship between SGV and loading plate bearing capacity is exponential whereas the walls maximum horizontal displacement is related to the second power of this variable.

4.5 Effect of doubling the plates of anchors

In this section, the breadth of the loading plate and back-to-back walls distances are kept constant and the bearing capacity of the loading plate, walls maximum horizontal displacements, and walls deformations are analyzed (Fig. 11).

It should be mentioned the single-plate anchors-related data -shown as dotted lines and hatched columns- are the old data from the author's previous studies that must be presented to compare to double-plate anchor cases (S letter at the beginning of the tests name show single-plate anchor cases).

A comparison of cylindrical diagrams of loading plate bearing capacity at its 5 cm settlement (Figs. 11(a) and 11(c)) shows that when walls are close (W=110 cm), doubling the plates of anchors leads to about a 5% decrease in loading plate bearing capacity on average whereas when walls are far from each other (W=140 cm) causes just 3% increase. This transforming process is visible in middle-range walls distances (W=120,130 cm). Also, it is presented for narrow loading plate (B=10 cm) when walls are close (W=110 cm) doubling the plate anchor causes increasing about 4%, whereas when walls are far from each other (W=140 cm) it causes decreasing about 4% in loading plate bearing capacity. Also, for a wide loading plate (B=50 cm), the relation of doubling the plates of anchors follows what was discussed for B=10 cm.

As the way, a comparison of the cylindrical graph of walls maximum horizontal displacements at 5 cm settlement of loading plate (Figs. 11(b) and 11(d)) shows that when walls are close (W=110 cm), doubling the plates of anchors leads to about 5% decrease of walls maximum horizontal displacement' on average whereas when walls are far from each other (W=140 cm) causes 3% increase. This behavior is seen in middle-range wall distances (W=120,130 cm). Also, the gradient of cylindrical graphs of the walls maximum horizontal displacements shows that when the loading plate is narrow (B=10 cm), doubling the plates of anchors almost leads to about a 5% decrease in walls horizontal displacement' on average whereas when walls are far from each other (W=140 cm) causes just 3%. This process is visible in middle-range wall distances (W=120,130 cm).

The deformation of walls demonstrated in Fig. 11(e) by walls horizontal displacements in three levels presents that doubling the plates of anchors leads to both curvature and tilting. But the comparison of their deformations presents that in single-plate anchored walls, rotation (tilting) is the dominant behavior whereas in double-plate anchored walls bending (curvature) is the dominant deformative behavior (both of them are shown in Fig. 12). These behaviors confirm that the rigidity of double-plate anchored walls is much more than single-plate anchored walls. This difference is very important for walls from a practical point of view. Since concrete walls are not suitable for resisting bending moments and reinforcing them or performing steel walls to achieve this goal can be expensive and time-consuming, therefore it is preferred to decrease the applied bending moment on these kinds of walls. Based on the results, doubling the plates of anchors can decrease the curvature and maximum bending moment accordingly (the bending moment is the differential of curvature $\frac{d\theta}{dx}$).

4.6 Slip surfaces (PIV)

One of the most important parameters in the design of retaining walls (like anchored walls) is the force applied to the wall by backfill. To determine and calculate the volume of the wall slip wedge and consequently its horizontal vector, specifying its form and shape is necessary. Therefore, in this study Photogrammetry and Particle Image Velocimetry (PIV) methods were used (Adrian 2005).

During each test, consecutive photos were taken from the backfill surface during deformation by a digital camera equipped with a CCD sensor, and soil deformations were evaluated between each pair of photos through the PIV analysis. To prevent camera displacement, all photos were provided by remote capture. Finally, images were analyzed through the PIV method using the GeoPIV module in MATLAB software. The output of this code is a two-dimensional matrix with u and v components, which represent horizontal and vertical components of the displacement vector in each point, respectively. This code was written by White *et al*. (2003) as an M-file in MATLAB software (White, Randolph, and Thompson 2005). Figs. 13 to 16 show the contours of shear strain (γ %) of soil particles in the critical composite surfaces for

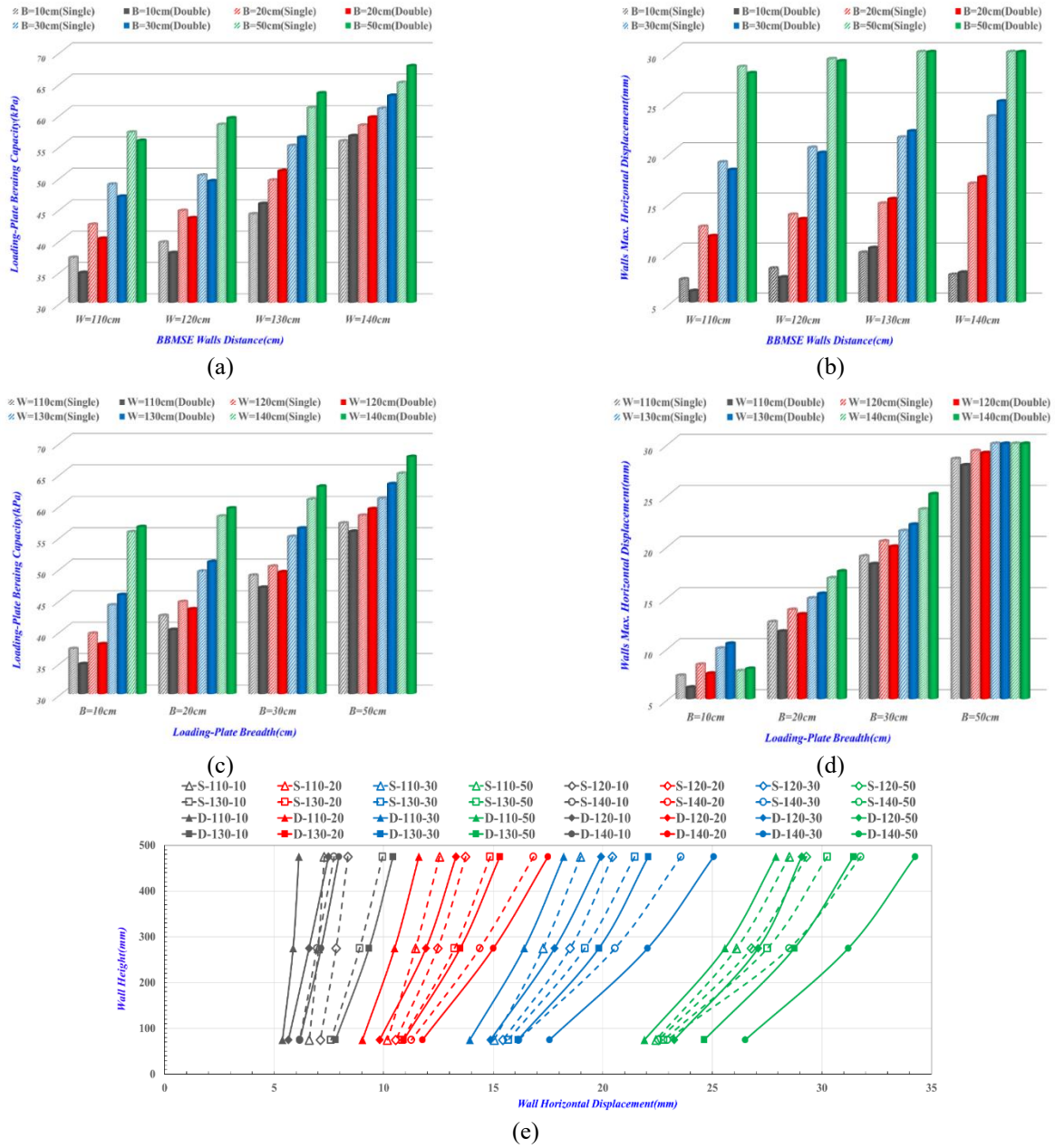

Fig. 11 Effect of doubling the plates of anchors on its bearing capacity, walls head displacements, and walls deformations

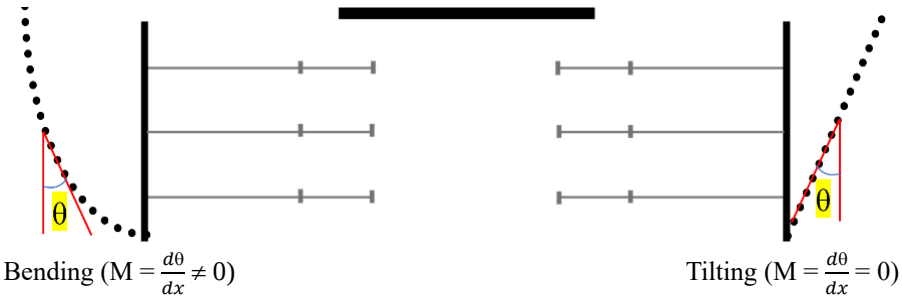

Fig. 12 Retaining walls deformations components

back-to-back anchored walls.

As mentioned above, in this composite of back-to-back anchored walls loaded by a shallow foundation, there are two slip failure surfaces of walls and one shear failuresurface of the shallow foundation (Fig. 6). The formation of each of them and its interaction with others

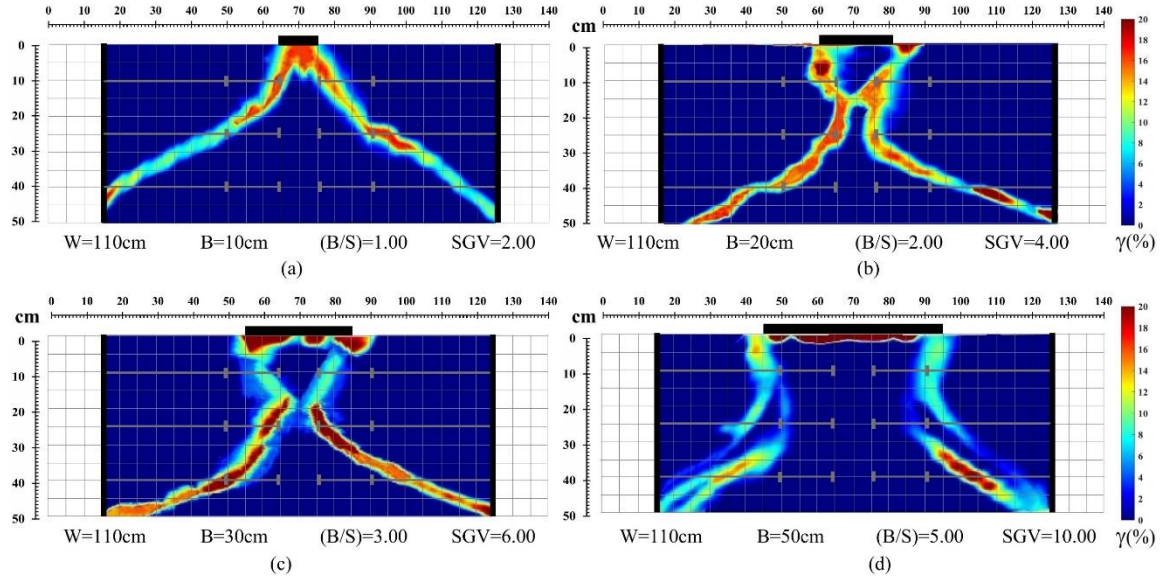

Fig. 13 Composite failure surface (PIV) of tests with W = 110 cm

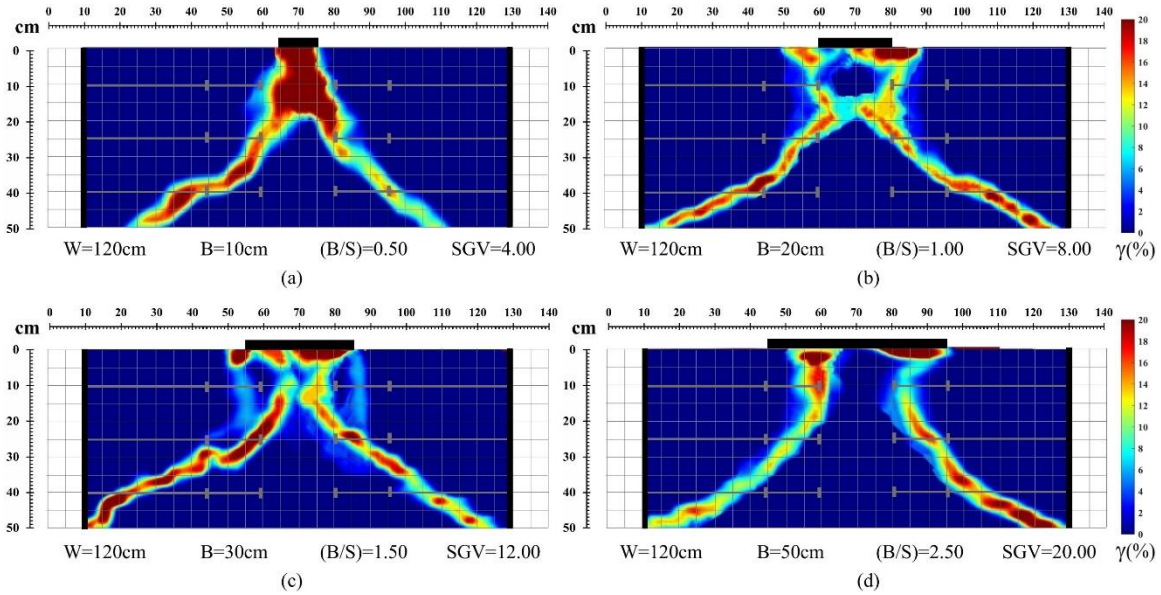

Fig. 14 Composite failure surface (PIV) of tests with W = 120 cm

can lead to different failure behavior and different form of the composite failure surface. Two composite modes of interactive failure (Mode I and Mode II) are seen in PIV output images as well.

Considering failure surfaces (PIV), when W=110 cm for B=10,20 cm (Figs. 13(a) and 13(b)) both of the walls composite failure surfaces are formed and superposed. Although for B=30 cm (Fig. 13(c)) walls slip failure surfaces are formed completely but superpose moderately. This behavior continues by increasing the loading plate breadth to B=50 cm (Fig. 13(d)) but for this loading plate, there is a special composite slip failure surface. Since this loading plate edge enters the internal slip failure surface, both internal and global slip failure surfaces are formed, but PIV results present that the global slip failure surface is more critical. Although in this case there is no unique composite failure surface. Due to this issue, in regression analysis of loading plate bearing capacity and walls maximum horizontal displacement with SGV the related data to D-110-50 and S-110-50 were removed from the procedure (Fig. 10). In the same way when in W=120 cm for B=10,20 cm (Figs. 14(a) and 14(b)) both of the walls composite failure surfaces are formed and superposed but for B=30 cm (Fig. 14(c)), walls composite failure surfaces are formed, partially though. Therefore, for this loading plate and wider (Fig. 14(d)), BBAW slip surfaces do not superpose and have interaction.

Also, when W=130 cm for B=10 cm (Fig. 15(a)) both of the walls composite failure surfaces superpose but are not formed completely. For B=20 cm (Fig. 15(b)), walls

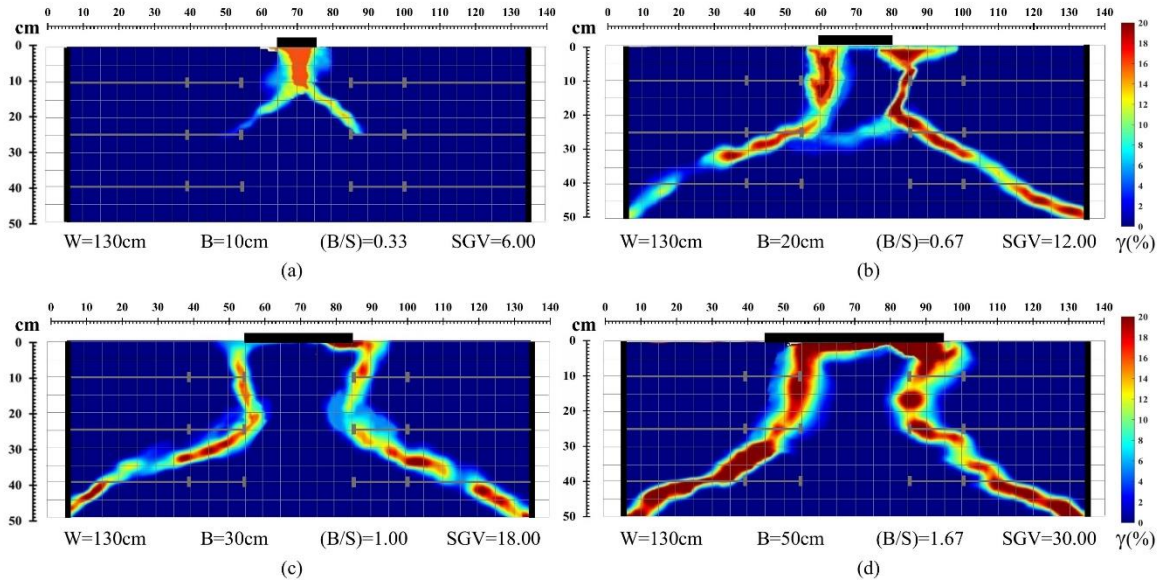

Fig. 15 Composite failure surface (PIV) of tests with W = 130 cm

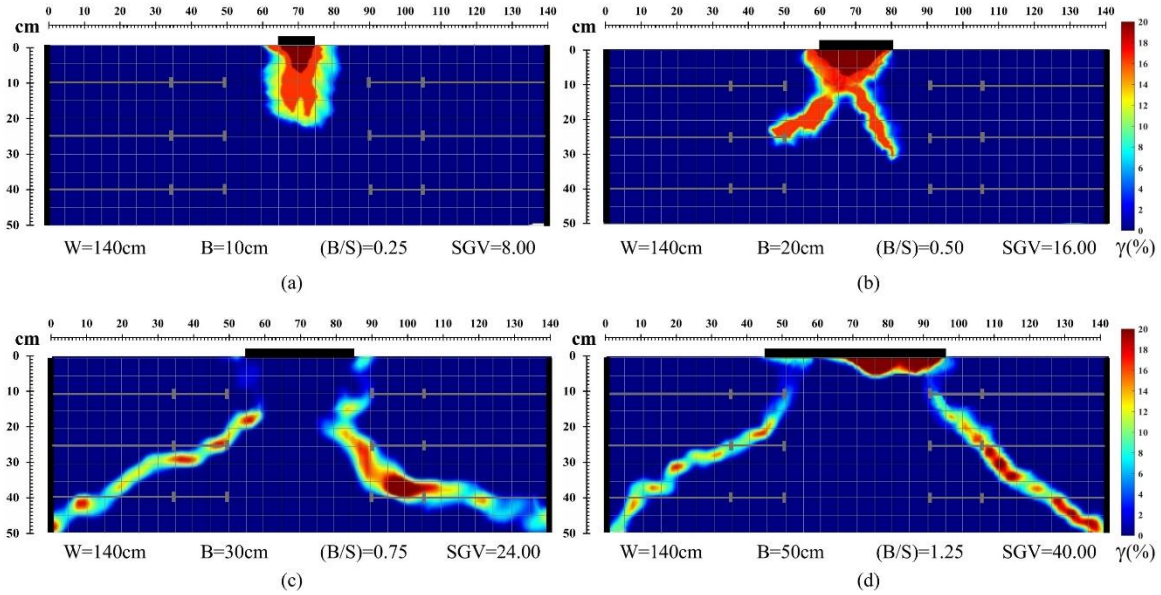

Fig. 16 Composite failure surface (PIV) of tests with W = 140 cm

composite failure surfaces are formed but interfere partially. In the same way, in this distance, for wider loading plates (Figs. 15(c) and 15(d)), BBAW composite failure surfaces do not superpose and have interaction. This situation continues when the distance of the walls till W=140 cm. In this distance of walls, for B=10 cm (Fig. 16(a)) the composite failure surfaces are not formed and do not superpose, at all and just shallow foundation shear failure surfaces are formed. Also, it is presented for B=20 cm (Fig. 16(b)) that composite failure surfaces cannot be formed completely until the toe of the walls. But for B=30,50 cm (Figs. 16(c) and 16(d)) composite slip surfaces are formed completely without interaction or superposition.

As was explained for all the distances of walls when the breadth of the loading plate is 50 cm or more, the composite failure surfaces do not interfere and interact, at all. therefore, the effective breadth is B=H and for this breadth and wider, the system failure Mode II (Fig. 6) does not occur and BBAW can be analyzed and designed singularly. Also, regarding slip failure surfaces (PIV), when B=10 cm in W=110,120 cm (Figs. 13(a) and 14(a)) both of the walls composite failure surfaces are formed and superpose but for W=130 cm (Fig. 15(a)) walls composite slip failure surfaces cannot be formed completely. This situation intensifies by increasing the distances of the walls to W=140 cm (Fig. 16(a)). At this distance of back-to-back walls, the slip surfaces of walls do not form, at all and therefore there is no composite failure surface.

As the way, when B=20 cm in W=110 cm (Fig. 13(b)) and somewhat W=120 cm (Fig. 14(b)) both walls composite

Table 4 Failure modes of back-to-back anchored retaining walls loaded by a limited-breadth surcharge

Test	B/S Ratio	System Geometry Variable (SGV)	Mode I Failure occurrence	Mode II Failure occurrence
D-110-10	1.00	1.00	Yes	Yes
D-110-20	2.00	2.00	Yes	Yes
D-110-30	3.00	3.00	Yes	Moderately
D-110-50	5.00	5.00	Yes	No
D-120-10	0.50	2.00	Yes	Yes
D-120-20	1.00	4.00	Yes	Yes
D-120-30	1.50	6.00	Yes	Partially
D-120-50	2.50	10.00	Yes	No
D-130-10	0.33	3.00	No	-
D-130-20	0.67	6.00	Yes	Partially
D-130-30	1.00	9.00	Yes	No
D-130-50	1.67	15.00	Yes	No
D-140-10	0.25	4.00	No	-
D-140-20	0.50	8.00	No	-
D-140-30	0.75	12.00	Yes	No
D-140-50	1.25	20.00	Yes	No

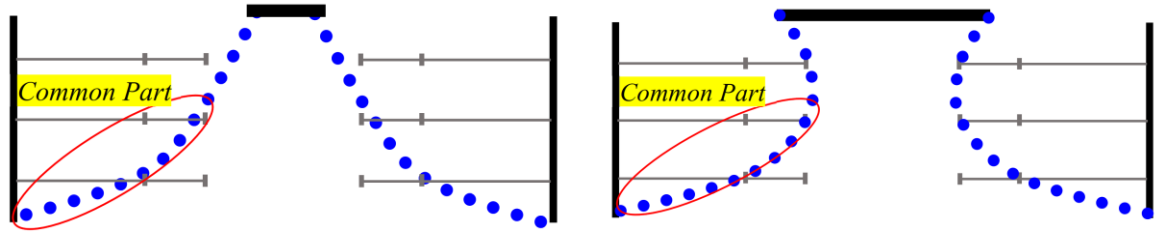

(a) (B/S) <1 (b) (B/S) >1

Fig. 17 Effect of B/S ratio on walls composite failure surfaces

slip failure surfaces are formed and superposed but when W=130 cm (Fig. 15(b)) BBAW composite failure surfaces cannot be formed completely until reach to walls toes. Therefore, at this distance and more, BBAW slip surfaces do not superpose and have interaction completely and this phenomenon is totally obvious for W=140 cm (Fig. 16(b)). Also, for B=30 cm in W=110 cm (Fig. 13(c)) and somewhat W=120 cm (Fig. 14(c)) the composite failure surface of walls slip failure surfaces and loading plate shear failure surface are formed and superpose altogether. But in W=130 cm (Fig. 15(c)) walls, composite failure surfaces are formed but do not interfere and superpose. Therefore, in this distance and more, BBAW composite failure surfaces do not superpose and have interaction. This phenomenon gets more obvious by increasing the distances of the walls to W=140 cm (Fig. 16(c)).

As explained, for B=50 cm in W=110 cm (Fig. 13(d)), both internal and global slip failure surfaces are formed. By Increasing the distances of walls internal slip failure surfaces are faded and in W=120,130,140 cm (Fig. 14(d) and 15(d) and 16(d)) just two composite failure surfaces are formed without interference or superpose.

Eventually, it is concluded that the effective distance of BBAW in this compound system is W =2.5*H and for longer distances, neither Mode I nor Mode II failures (Fig. 6) happen and then there is no interacted zone among the two walls, and loading plate.

Also, regarding the effect of the S/B ratio on composite failure surface, as was shown in Fig. 17, apart from the common part (The PIV results showed that in most of the tests, composite failure surface passes through two points directly. The first point is middle plate anchors and the second is walls toes (Fig. 17)), when (B/S) <1 (Fig. 17(a)), composite failure surface does not pass through top plate anchors, but when (B/S) >1(Fig. 17(b)) it passes through that. This phenomenon is very important because in the first case (Fig. 17(a)) with increasing the S/B ratio the top plate anchors are going to lose their acts in walls external stabilities.

In summary, the PIV results show that the incidents of explained failure modes in tests are presented in Table 4.

Moreover, from other results of PIV analysis other deformations and displacements can be achieved like Vectorial Displacement, Resultant Contours, Horizontal Contours, Vertical Contours, etc (White *et al*. 2001, 2003, 2005). As some samples, the graphical results that can be accessed from PIV analysis of test D-140-30, are shown in Fig. 18. These outputs were used to enrich the analysis of

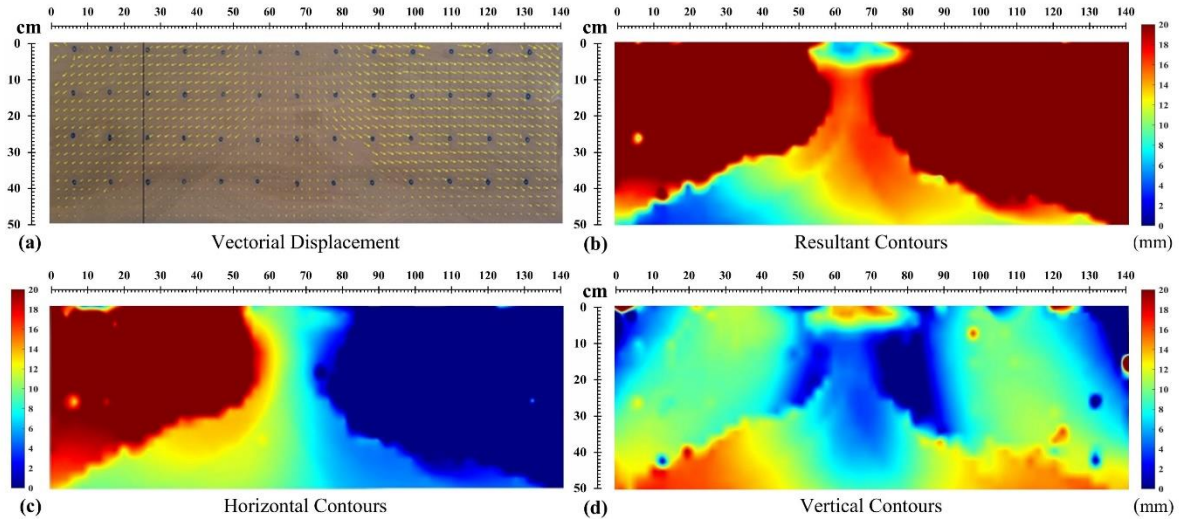

Fig. 18 PIV results of the D-140-30 test

this study but considering the limitations of this article, showing all of those for all the tests is impossible.

As mentioned, the S/B ratio is an indicator of the intensity of interactive behavior among the components of the compound system. As is seen in Fig. 18, in test D-140-30 (B/S=0.75) dominance of horizontal displacements on vertical displacements as a result of interactions is inferable and obvious. But with decreasing the B/S ratio the vertical displacement goes to be dominant. This issue as discussed, for D-140-10 (B/S=0.25), is presented in Fig. 17(a) that shows because B/S is very small the walls do not sense and activate by forcing and settlement of the loading plate.

5. Conclusions

- The compound system including two back-to-back anchored walls (BBAW) loaded by limited-breadth load (like a shallow foundation) cannot be analyzed and designed in the singular analysis mode of each part. In this system, there are two kinds of interference and interaction. The first is a composite of a wall external slip surface and shallow foundation shear surface and the second is interference and interaction of two composite failure surfaces.
- Increasing the distance of BBAW (W) -loaded by a shallow foundation- leads to an increase in shallow foundation bearing capacity and walls horizontal displacements. The effective distance is W/H=2.5 (H= height of back-to-back walls) and for longer distances, the walls composite failure surfaces do not interact with each other and can be analyzed and designed individually.
- Increasing the breadth of shallow foundation (B) of -load on two BBAW- causes to increase in its bearing capacity and walls horizontal displacements. The effective breadth is B=H (H= height of back-to-back walls) and for this breadth and wider foundations, the walls composite failure surfaces do not interfere with each other and can be analyzed and designed singularly.
- In practical cases, when there is a limitation in walls distances or shallow foundation breadth, considering the walls effective distance and the foundation effective breadth, one may use another parameter to prevent the formation of a compound system (Walls and shallow foundation) from interfering and interactions.
- Doubling the plates of anchors, in some cases of BBAW -loaded by the shallow foundation- leads to an increase of the shallow foundation bearing capacity and walls horizontal displacements and, in some cases, vice versa. The important influence of doubling the plates of anchors is decreasing the curvature of the wall by transforming it into displacement. This feature facilitates using concrete walls that have limitations in tolerating curvature.
- There is a direct relationship between the S/B ratio (the ratio of two BBAW plate anchors' distances to loading plate breadth that presents the position of the load relative to walls) and system interactive behavior that influences foundation bearing capacity and walls horizontal displacement. Moreover, PIV results showed when the S/B<1, the top series of plate anchors do not act in stabilizing BBAW.
- There is an exponential relation between the System Geometry Variable (SGV) of BBAW -loaded by the shallow foundation- and the shallow foundation bearing capacity and the second power of this Variable to walls maximum horizontal displacements.

References

Adrian RJ. (2005), "Twenty years of particle image velocimetry", *Exp. Fluids*, **39**(2): 159-169. https://doi.org/10.1007/s00348-005-0991-7

ASTM D1194-94 (Withdrawn 2003), *Standard Test Method for Bearing Capacity of Soil for Static Load and Spread Footings*,

ASTM International, West Conshohocken, USA, 1994. Available: https://www.astm.org/d1194-94.html.

ASTM D3080-04 (2004), *Standard test method for the direct shear test of soils under consolidated drained conditions,* American Society for Testing and Materials, West Conshohocken, USA: ASTM International. Available: https://www.astm.org/d3080-04.html.

Benmebarek, S. and Djabri, M. (2017), "FE analysis of back-to-back mechanically stabilized earth walls under cyclic harmonic loading", *Indian Geotech. J.*, **48,** 498-509, https://doi.org/10.1007/s40098-017-0269-z.

Das, B.M. and Shukla, S.K. (2014), "Earth anchors", 2nd Ed., J. Ross Publishing, Inc, Florida, USA.

El-Sherbiny, R., Ibrahim, E. and Salem, A. (2013), "Stability of back-to-back mechanically stabilized earth walls", *Proceedings of the Geo-Congress 2013 (Stability, and Performance of Slopes and Embankments III)*. https://doi.org/10.1061/9780784412787.058.

Han, J. and Leshchinsky, D. (2010), "Analysis of back-to-back mechanically stabilized earth walls", *Geotext. Geomembranes*, **28**, 262-267, https://doi.org/10.1016/j.geotexmem.2009.09.012.

Jalali Moghaddam, M., Dastaran, N. and Zad, A. (2021), "Introducing expandable mechanical plate anchors for onshore and offshore anchoring", *J. Marine Georesour. Geotech.* ,**40**(3), 329-348, https://doi.org/10.1080/1064119X.2021.1894274.

Jalali Moghaddam, M., Zad, A., Mehrannia, N. and Dastaran, N. (2019), "Experimental study on the performance of plate anchor retaining walls", *Int. J. Phys. Model. Geotech.*, **19** (3), 128-140. https://doi.org/10.1680/jphmg.17.00040.

Lazarte, C.A., Robinson, H., Gómez, J.E., Baxter, A., Cadden, A. and Berg, R. (2015), *Soil nail walls reference manual*, Report No. FHWA-NHI-14-007. Department of Transportation, Federal Highway Administration, Washington, USA.

Moghadam, M.J., Zad, A., Mehrannia, N. and Dastaran, N. (2018), "Experimental evaluation of mechanically stabilized earth walls with recycled crumb rubbers", *J. Rock Mech. Geotech. Eng.*, **10**(5), 947-957. https://doi.org/10.1016/j.jrmge.2018.04.012.

Najafizadeh, A., Zad, A.A. and Yazdi, M. (2022), "Experimental evaluation of back-to-back anchored walls by single plate anchors", *Int. J. Geomech.*, **22**(12). https://doi.org/10.1061/(asce)gm.1943-5622.0002470.

Niroumand, H. and Kassim, K.H. (2016), *Design and Construction of Soil Plate anchors* (1st Ed.), Elsevier Science, Amsterdam, Netherland.

Perko, H.A. (2009), *Helical piles: a practical guide to design and installation*. John Wiley and Sons, Hoboken, New Jerse, USA.

Ryan, R. Berg, Barry R. Christopher, and Naresh C. Samtani, (2009), *Mechanically Stabilized Earth Walls and Reinforced Soil Slopes – Volume I*, Report No. FHWA- NHI-10-024, Federal Highway Administration, U.S. Department of Transportation, Washington, DC.

Sabatini, P., Pass, D. and Bachus, R.C. (1999), *Ground Anchors and Anchored Systems,* Geotechnical engineering circular No. 4:. Report No. FHWA-IF-99-9015. Department of Transportation, Federal Highway Administration, Washington, USA..

Taghizadeh, S., Nazari Afshar, J., and Zad, A. (2016), "FE analysis of external and internal stability of back-to-back mechanically stabilized earth walls", Thesis for M.Sc. Islamic Azad University (in Persian), Tehran, Iran.

Terzaghi, K. (1943), *Theoretical soil mechanics*, John Wiley and Sons Inc, 5th ed., New York, N.Y.

Tognon, A.R., Rowe, R.K. and Brachman, R.W. (1999), "Evaluation of side wall friction for a buried pipe testing facility", *Geotext. Geomembranes*, **17**(4), 193-212. https://doi.org/10.1016/S0266-1144(99)00004-7.

White, D., Randolph, M., and Thompson, B. (2005), "An image-based deformation measurement system for the geotechnical centrifuge", *Int. J. Phys. Model. Geotech.*, **5**(3), 1-12. https://doi.org/10.1680/ijpmg.2005.050301.

White, D., Take, W. and Bolton, M. (2003), "Soil deformation measurement using particle image velocimetry (PIV) and photogrammetry", *Geotechnique*, **53**(7), 619-631. https://doi.org/10.1680/geot.2003.53.7.619.

White, D., Take, W., and Bolton, M. (2001), "Measuring soil deformation in geotechnical models using digital images and PIV analysis", *Proceedings of the 10th international conference on computer methods and advances in geomechanics*, Rotterdam: A.A. Balkema.

Won M.S. and Kim, Y.S., (2007), "Internal deformation behavior of geosynthetic-reinforced soil walls", *Geotext. Geomembranes*, **25**, 10-22. https://doi.org/10.1016/j.geotexmem.2006.10.001.

Wood David, M. (2004), Geotechnical modeling, Routledge, (Version 2.2), London, England.

JS